Catalysis Today 141 (2009) 409–414

Contents lists available at ScienceDirect

Catalysis Today

journal homepage: www.elsevier.com/locate/cattod

Comparative study of the reducibility under H_2 and CO of two thermally aged $Ce_{0.62}Zr_{0.38}O_2$ mixed oxide samples

María P. Yeste, Juan C. Hernández, Serafín Bernal *, Ginesa Blanco, José J. Calvino, José A. Pérez-Omil, José M. Pintado

Departamento de Ciencia de Materiales e Ingeniería Metalúrgica y Química Inorgánica, Facultad de Ciencias, Universidad de Cádiz, Campus Río San Pedro, E-11510 Puerto Real (Cadiz), Spain

ARTICLE INFO

Article history:
Available online 9 June 2008

Keywords:
Ceria-zirconia
Thermal ageing
Redox behaviour
H_2-OSC
CO-OSC

ABSTRACT

The redox behaviour under flowing 5%CO/He and 5%H_2/Ar of two $Ce_{0.62}Zr_{0.38}O_2$ mixed oxides is investigated. The samples, hereafter referred to as CZ-MO and CZ-SO, were obtained by application to the same starting material two well established thermal ageing routines. These routines ensured the preparation of oxide samples with significantly different chemical and structural properties. To evaluate their redox behaviour, ultimate oxygen storage capacity (OSC) data were determined from stepwise thermo-gravimetric experiments at temperatures ranging from 473 K to 1173 K. In good agreement with earlier studies from the literature, both CO-OSC and H_2-OSC data show that CZ-MO exhibits a superior reducibility throughout the whole range of temperatures. If CO-OSC and H_2-OSC data are compared, we may notice that, in qualitative agreement with the thermodynamic predictions, CO-OSC values are significantly larger than those of H_2-OSC at $T \leq 773$ K. Above this reference temperature CO-OSC and H_2-OSC show much closer values. Though ultimate OSC data are generally assumed to be determined by the thermodynamics of the oxide-reductant system, it is shown that the CO-OSC values recorded at the lowest temperatures are not consistent with this assumption. As in the case of H_2-OSC, the low-temperature CO-OSC data are actually determined by kinetic factors.

1. Introduction

Ceria-zirconia mixed oxides are highly interesting materials with a variety of relevant applications [1]. Catalysis is probably the field in which some of the most successful large-scale uses of these oxides may be found [2–4]. The three-way catalysts (TWC) for the abatement of exhaust emissions from gasoline-fuelled automobiles is an outstanding example of it. In effect, as several authors have stressed [5–7], the incorporation of ceria-zirconia mixed oxides to the TWC formulation, in the mid-1990s, has represented a major breakthrough point in the development of this technology. More recently, several other catalytic uses in automotive soot oxidation [8–10], water pollution control [11], or in reactions like water gas shift [12–15], or selective oxidation of CO in presence of a large excess of H_2 [16–18], key processes in hydrogen generation for fuel cell applications, are being explored. In all these applications, the redox behaviour of the ceria-zirconia mixed oxides is acknowledged to play a relevant role. In accordance with this, the evaluation of their oxygen exchange capability is a major objective in the chemical characterization of these materials [2] As discussed in [19], a large variety of chemical, spectroscopic and magnetic techniques have been applied to the redox characterization of ceria and ceria-based mixed oxide materials. Among them, the chemical techniques, and more specifically, the temperature programmed reduction (TPR) [20–23] and the so-called oxygen storage capacity (OSC) measurements [24–32] are by far the experimental studies most commonly reported in the literature.

At least two different types of measurements are generally included under the acronym OSC [20,24,33]. Ultimate, total, or complete OSC is aimed at determining the highest amount of oxygen that may be exchanged by the investigated material under certain pre-established conditions. It is generally assumed that this parameter reflects thermodynamic properties of the oxide [33]. From the experimental point of view, ultimate OSC data are usually obtained either gravimetrically [26], i.e. by measuring the weight loss undergone by the oxide after prolonged contact with the reducing agent at a certain temperature and partial pressure of it; or by volumetric determination of the oxygen consumed by the pre-reduced material [23,25]. Hydrogen and carbon monoxide are the most commonly used reductants [24].

The objective of the dynamic or kinetic OSC measurements, on the contrary, is the evaluation of the most reactive oxygen species.

* Corresponding author.
E-mail address: serafin.bernal@uca.es (S. Bernal).

0920-5861/$ – see front matter © 2008 Elsevier B.V. All rights reserved.
doi:10.1016/j.cattod.2008.04.023

For this purpose, the response of the investigated materials is investigated under transient conditions, either by short pulses of the reductant (typically H_2 or CO), or by alternating H_2(CO)/O_2 pulses [24,27,29,32].

In this work we shall focus our attention on ultimate OSC measurements. In spite of their generalized use, the variety of experimental conditions (temperature, nature and partial pressure of the reducing agent, and time of reduction) and investigated materials make very difficult the meaningful comparison of data from different laboratories. For this reason, it seemed interesting to us the determination and comparative analysis of ultimate H_2-OSC and CO-OSC recorded in a wide range of temperatures for two well characterized ceria-zirconia samples. The experimental routine followed throughout the whole series of measurements was always the same. As will be shown, in the low-temperature range ($T \leq 773$ K), remarkable differences are observed between CO-OSC and H_2-OSC data, they becoming much closer at the highest investigated temperatures ($T \geq 973$ K). The role of both thermodynamic and kinetic factors in determining the reported OSC values and its evolution with the temperature of measurement is discussed.

2. Experimental

Two $Ce_{0.62}Zr_{0.38}O_2$ mixed oxide samples have been investigated. They will be referred to as CZ-MO and CZ-SO, respectively. They were prepared as reported in [25]. In brief, two aliquots of a commercial, low surface area (S_{BET}: 19 $m^2\ g^{-1}$), $Ce_{0.62}Zr_{0.38}O_2$ sample, were reduced in a flow of pure hydrogen at 1223 K 5 h), flushed with He, at 1223 K (1 h), and then cooled to 298 K under inert gas flow. Two different re-oxidation routines were further applied to them. One of the reduced aliquots was first pulsed with O_2(5%)/He, then heated in a flow of O_2(5%)/He at 773 K (1 h), and finally cooled to 298 K under the same oxidizing mixture, mild oxidation treatment (MO), thus resulting the CZ-MO sample (S_{BET}: 16 $m^2\ g^{-1}$). The other one was re-oxidized in a flow of pure O_2 at 1223 K (5 h), followed by cooling to 298 K under the same flow, severe oxidation treatment (SO). In this way the so-called CZ-SO sample (S_{BET}: 12 $m^2\ g^{-1}$) was obtained.

The reported powder X-ray diffraction diagrams (XRD) patterns were recorded on a Bruker AXS, D8 Advance, instrument, under the following conditions: Cu Kα radiation, step: 0.05°, and the time per step: 30 s.

HREM images were recorded on a JEOL 2010-FEG instrument with a structural resolution of 0.19 nm. The digital diffraction patterns (DDPs) reported as insets in the HREM figures correspond to the log-scale power spectrum of the corresponding fast Fourier transform. Differential thermo-gravimetric studies (CO-DTG, H_2-DTG) were run on a TA thermo-balance, model Q-600. Typically, the weight of oxide sample was 100 mg. The flow rate of either 5%CO/He or 5%H_2/Ar was 60 $cm^3\ min^{-1}$, and the heating rate 10 K min^{-1}. Prior running all these experiments, the oxides were heated in flow of 5%O_2/He at 773 K (1 h), and further cooled to 398 K under the same gaseous mixture; then the gas flow was switched to He, and finally to the reducing gaseous mixture.

Ultimate OSC data were determined by stepwise thermogravimetric analysis. The samples were pre-treated by following the same protocol described above for the continuous DTG experiments. After completing the pre-treatment routine, at 398 K, the gas flow was switched to 60 $cm^3\ min^{-1}$ of 5%CO/He (5%H_2/Ar), and started the stepwise reduction experiment. The heating rate between successive isothermal steps was 10 K min^{-1}, and the time at each of these steps 1 h.

3. Results and discussion

3.1. Structural characterisation studies

Figs. 1 and 2 summarise the structural characterisation studies carried out on the CZ-MO and CZ-SO samples. Both XRD diagrams (Fig. 1) and HREM images (Fig. 2) are fully consistent with earlier studies on the nano-structural constitution of the two samples above [25,34,35]. In accordance with them, CZ-MO sample exhibits some very specific super-structure features (see the HREM contrasts corresponding to lattice spacings double than those of the primitive fluorite-type structure in Fig. 2b, as well as the characteristic XRD peak observed in the low angle region reported in the inset of Fig. 1b, and the digital diffraction pattern (DDP) also included as inset in Fig. 2b) which have been interpreted as due to an ordered arrangement in the cationic sub-lattice similar to that observed in the pyrochlore-type phases [35]. On the contrary, the XRD, HREM and DDP data reported, respectively, in Figs. 1a and 2a suggest that, for the CZ-SO sample, the ordering effect induced by the high-temperature reduction followed by the mild re-oxidation treatment in the CZ-MO oxide, is now destroyed as a result of the high-temperature oxidation conditions applied to it in the second step of the preparation routine [25]. These structural differences have a dramatic effect on the redox response against H_2 of CZ-MO and CZ-SO samples [25].

3.2. Temperature programmed reduction studies

Figs. 3 and 4 show, respectively, the CO-DTG and H_2-DTG traces recorded for CZ-MO and CZ-SO samples. There are a number of points to be outlined in connection with these experiments. Regarding the H_2-DTG (Fig. 3) we may notice that the reduction of CZ-MO starts at significantly lower temperatures than that of CZ-SO. This observation is in fairly good agreement with the results of the H_2-TPR-MS study carried out on the same oxide samples [25].

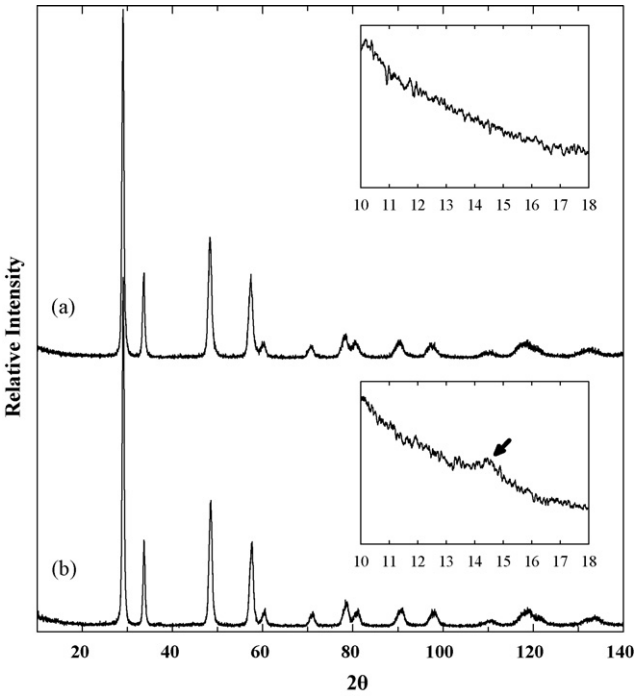

Fig. 1. X-ray powder diffraction study of CZ-SO (a) and CZ-MO (b) samples. The insets show enlarged diagrams of the 2θ range at which the super-structure peak characterising the occurrence of ordering in the cationic sub-lattice (pyrochlore-related phase) is observed.

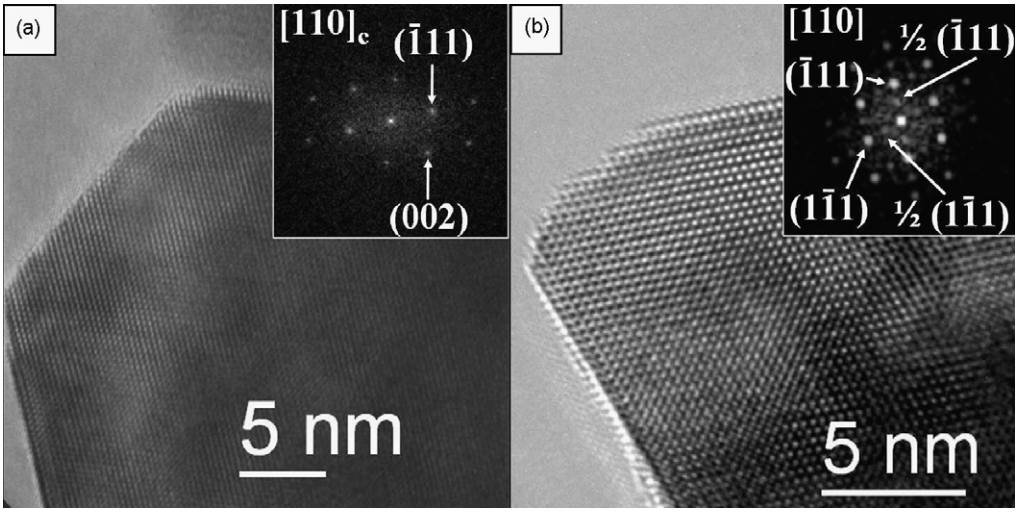

Fig. 2. Representative HREM images for CZ-SO (a) and CZ-MO (b) samples. The corresponding digital diffraction patterns (DDPs) generated from the images are shown as insets.

As discussed in [25], though significant differences may be noted between the thermodynamics of CZ-MO and CZ-SO reduction, their low-temperature behaviour is considered to be determined by the kinetics of the dissociative chemisorption of hydrogen on them. This reaction, which is considered to control the rate of the overall reduction process for $T \leq 773$ K, was shown to be faster on the CZ-MO sample [25].

The low-temperature redox response of CZ-MO and CZ-SO under flowing 5%CO/He should also be commented on. In qualitative agreement with their behaviour against 5%H_2/Ar, the reducibility of the CZ-MO sample is significantly higher than that of the CZ-SO. As in the case of the H_2 reduction study, the question is whether the difference of low-temperature reducibility deduced from the comparison of a and b CO-DTG diagrams in Fig. 4 is due to thermodynamic or kinetic factors. This point will be discussed to some extent below.

The comparative analysis of the results reported in Fig. 3 (H_2-DTG) and Fig. 4 (CO-DTG) also deserves some comments. With reference to the corresponding H_2-DTG traces, the main reduction peak in the CO-DTG diagrams is significantly shifted towards lower temperatures. We should conclude, accordingly, that, for both oxide samples, the low-temperature reducibility under flowing 5%CO/He is higher than that observed in flow of 5%H_2/Ar. From a thermodynamic point of view, for temperatures below 900 K, the reducing power of CO is superior to that of the H_2, the difference progressively increasing as the temperature decreases. Accordingly, in the low-temperature range, CO should be expected to be a more effective reductant than H_2. Again, the question arising is whether the recorded CO-DTG traces are mainly determined by thermodynamic factors, or the kinetic aspects of the process must also be considered in the interpretation of these diagrams. The analysis of the OSC data reported below will shed some light on this issue.

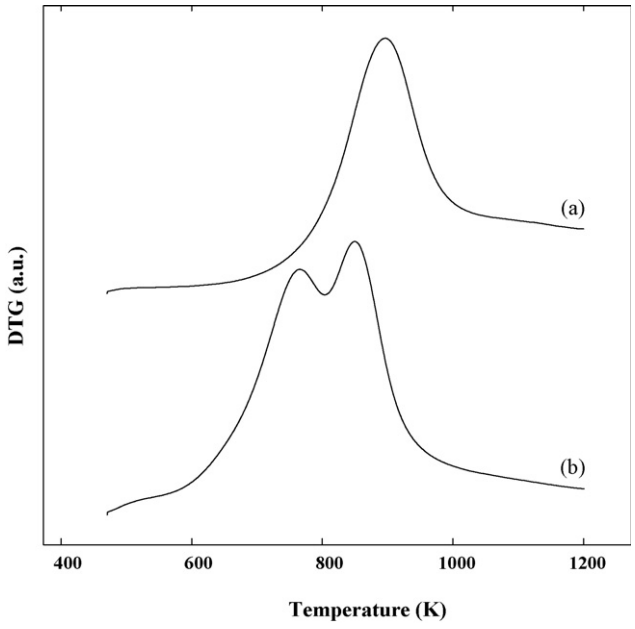

Fig. 3. DTG diagrams corresponding to the reduction in flow of 5%H_2/Ar of CZ-SO (a) and CZ-MO (b). Heating rate: 10 K min^{-1}. Prior running the experiments, the oxides were heated under flowing 5%O_2/He at 773 K (1 h).

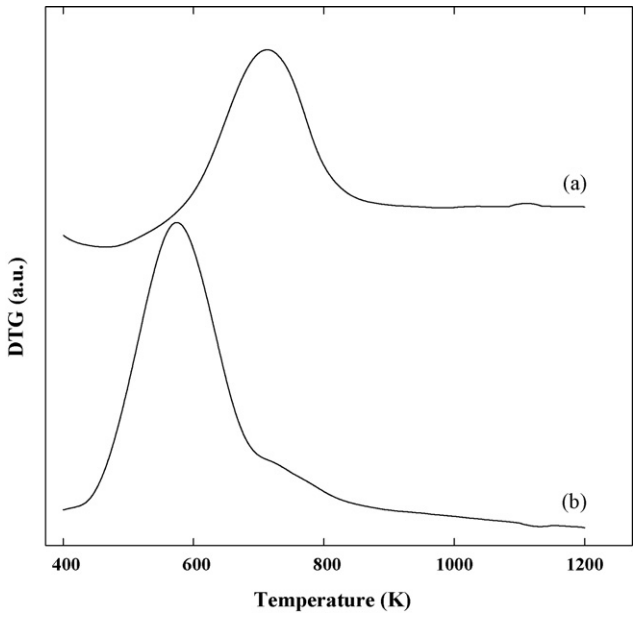

Fig. 4. DTG diagrams corresponding to the reduction in flow of 5%CO/He of CZ-SO (a) and CZ-MO (b). Heating rate: 10 K min^{-1}. Prior running the experiments, the oxides were heated under flowing 5%O_2/He at 773 K (1 h).

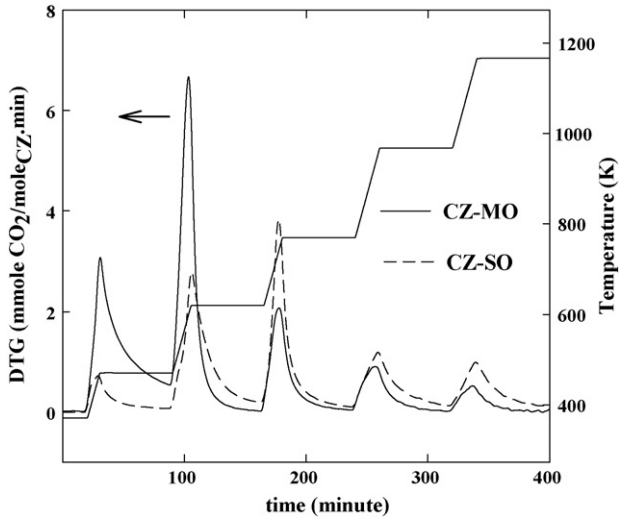

Fig. 5. Ultimate CO-OSC study. DTG traces corresponding to the stepwise reduction of CZ-MO (full line) and CZ-SO (dotted line) in a flow of 5%CO/He. Heating rate between successive steps: 10 K min^{-1}. Duration of the isothermal steps: 1 h. Prior running the experiments, the oxides were heated under flowing 5%O_2/He at 773 K (1 h).

3.3. Ultimate oxygen storage capacity (OSC) measurements

Figs. 5 and 6 show, respectively, the CO-DTG and H_2-DTG diagrams recorded in the stepwise thermo-gravimetric study of the reduction of CZ-MO and CZ-SO samples. From the analysis of these experiments, ultimate CO-OSC and H_2-OSC data for temperatures ranging from 473 K to 1173 K could be determined. These results are reported in Table 1.

We have also run a stepwise H_2-DTG experiment on a Rh(0.3 wt.%)/CZ-MO (Fig. 7). This sample is the same as that earlier investigated in [25]. Table 1 also includes the series of ultimate H_2-OSC values determined from the DTG experiment reported in Fig. 7, as well as those taken from [25] for a Rh(0.3%)/CZ-SO sample. This latter series of data were determined from volumetric chemisorption of O_2 [25]. As will be discussed below, this additional information on Rh-modified oxides provides with very useful references for the analysis of the results reported in Figs. 5 and 6.

Table 1
Ultimate CO-OSC and H_2-OSC data expressed as percentage of total Ce^{4+} reduced to Ce^{3+}

Sample/reductant	Ultimate OSC (% of Ce^{4+} reduced to Ce^{3+})				
	473 K	623 K	773 K	973 K	1173 K
CZ-MO/CO[a]	28	59	72	79	83
CZ-MO/H_2[a]	3	28	64	77	83
0.3 wt.%Rh/CZ-MO/H_2[a]	45	55	65	75	82
CZ-SO/CO[a]	5	27	47	59	69
CZ-SO/H_2[a]	0	2	22	55	70
0.3 wt.%Rh/CZ-SO/H_2[b]	23	31	39	–	67

[a] Data as determined in this work from stepwise TG experiments.
[b] Data taken from ref [25]. They were obtained from O_2 volumetric adsorption at 473 K.

To facilitate the comparative analysis of the OSC data reported in Table 1, the most relevant part of them have also been plotted in Fig. 8.

As deduced from Table 1 and Fig. 8, both OSC-H_2 and OSC-CO data show that, throughout the whole range of investigated temperatures, the reduction degrees reached by the CZ-MO sample are higher than those of the CZ-SO. This observation is in full agreement with the results reported in some earlier studies [25,26,36], in accordance with which, the thermally aged oxides exhibiting an ordered Ce-Zr sub-lattice, i.e. the CZ-MO sample in the present case, show an enhanced thermodynamic reducibility. This is a consequence of the change occurred in the relative thermodynamic stability of the ordered and disordered structures as a function of the redox state of the samples. Under oxidising conditions, the higher stability corresponds to the phase showing a disordered arrangement in the cationic sub-lattice, i.e. to the CZ-SO sample, whereas the opposite is true for the oxides in their reduced state [25,36].

The comparative analysis of the CO-OSC and H_2-OSC data recorded for CZ-MO and CZ-SO does also deserve some comments. For the same oxide sample, in the low-temperature range ($T \leq 773$ K), OSC-CO values are significantly larger than those of

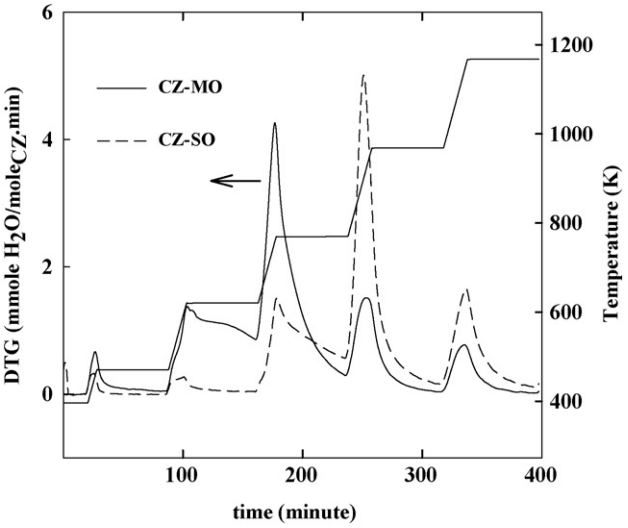

Fig. 6. Ultimate H_2-OSC study. DTG traces corresponding to the stepwise reduction of CZ-MO (full line) and CZ-SO (dotted line) in flow of 5%H_2/Ar. Heating rate between successive steps: 10 K min^{-1}. Duration of the isothermal steps: 1 h. Prior running the experiments, the oxides were heated under flowing 5%O_2/He at 773 K (1 h).

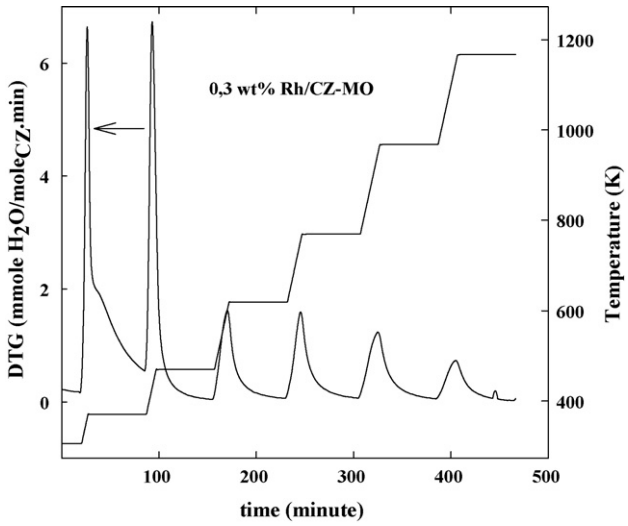

Fig. 7. Ultimate H_2-OSC study. DTG traces corresponding to the stepwise reduction of Rh(0.3%)/CZ-MO in a flow of 5%H_2/Ar. Heating rate between successive steps: 10 K min^{-1}. Duration of the isothermal steps: 1 h. Prior running the experiments, the oxides were heated under flowing 5%O_2/He at 773 K (1 h).

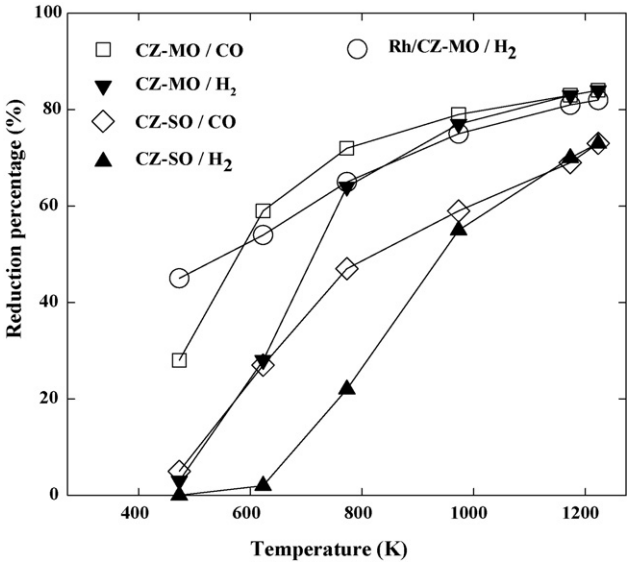

Fig. 8. Evolution with the temperature of ultimate CO-OSC and H_2-OSC data for CZ-SO and CZ-MO. H_2-OSC data for Rh/CZ-MO are also included for comparison. OSC is expressed as percentage of Ce^{4+} reduced to Ce^{3+}.

OSC-H_2. By contrast, for $T \geq 973$ K, much closer values are experimentally observed. This is in qualitative agreement with the variation of ΔG_r^o for CO and H_2 oxidation reactions against T. As shown in Fig. 9, the slope of the approximately linear plot $\Delta G_r^o - T$, is higher for the former reaction, the crossing point occurring at approximately 900 K. For $T < 900$ K, the relative reducing power of CO progressively increases with respect to that of the H_2, as the temperature decreases. On the contrary, above 973 K, H_2 would be slightly more effective. If this effect is combined with the evolution of the thermodynamic parameters for the reduction of the oxides with their redox state [37], we may understand the general trends followed by the CO-OSC and H_2-OSC data as the temperature is increased.

As shown in Fig. 9, the largest differences between CO-OSC and H_2-OSC data are found at $T \leq 773$ K. If we focus our attention on this domain of Fig. 8, some remarkable observations can be made. For kinetic reasons, in flow of H_2, the low-temperature reducibility of the oxides is strongly enhanced by the presence of small amounts of Rh supported on them [25]. Assuming that the rhodium phase does not modify the thermodynamic properties of the oxides, the dramatic

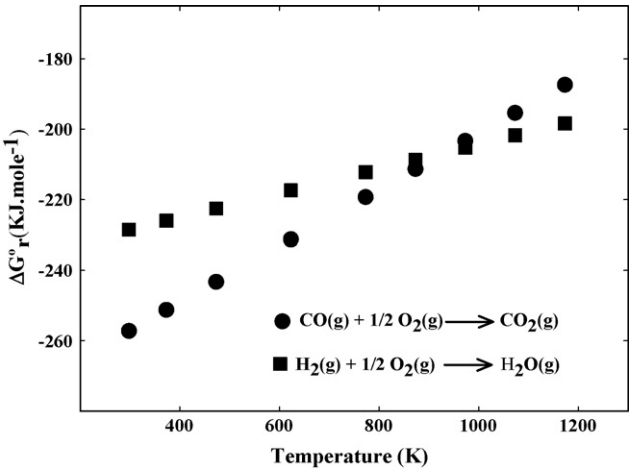

Fig. 9. ΔG_r^o versus T plots for CO and H_2 oxidation reactions.

influence of the metal should be interpreted as due to a catalytic effect. On rhodium, H_2 adsorption would be faster, thus favouring the subsequent transfer of atomic hydrogen to the support *via spillover*. If so, the H_2-OSC value determined for the Rh-containing samples would actually provide oxygen storage data much closer to the thermodynamic limit of the oxide reduction than those for the bare oxides, at the same temperature. This is a relevant observation. In effect, if H_2-OSC data reported in Table 1 for Rh/CZ-MO and Rh/CZ-SO are compared with those of CO-OSC for the corresponding bare oxides, we may notice that, at 473 K, the former are much larger than the latter. As already discussed, this is unexpected from the thermodynamic point of view. Actually, in accordance with Fig. 9, if a true equilibrium state would have been reached, at 473 K, CO-OSC data should be larger than the corresponding H_2-OSC values. Therefore, as in the case of the H_2-OSC values determined from either volumetric studies [25], or the gravimetric measurements reported in this work, for the bare oxides, the CO-OSC data recorded at the lowest temperatures are determined by kinetic rather than thermodynamic factors. This conclusion is also supported by the shape of the stepwise CO-DTG diagrams in Fig. 5. As clearly shown in the first step of the CO-DTG trace for CZ-MO in Fig. 5, after 1 h isothermal heating at 473 K, the rate of reduction is still measurable, i.e. the equilibrium reduced state could not be reached at the end of this isothermal step. The same is true for CZ-SO even at 623 K, which suggests that the kinetic restrictions are even stronger on this sample. The latter proposal is also supported by the remarkable upwards shift of the main peak in the continuous CO-DTG trace for CZ-SO (Fig. 4a) as compared to that for CZ-MO (Fig. 4b).

Additional studies are currently under way to fully understand the origin of the observed kinetic control in ultimate CO-OSC measurements. It would be noted, however, that, in accordance with the results reported in Table 1 for the oxide-supported Rh samples, the oxygen diffusion step is unlikely to be the rate controlling step of the overall reduction process under flowing CO. Therefore, the kinetic control is probably associated to either the CO adsorption step leading to the formation of carbonate species [38], or to the subsequent decomposition of the above mentioned carbonates. Some recent studies on the mechanism of CO oxidation over ceria-zirconia under dynamic conditions [29,38] allow us to suggest that the decomposition of the surface carbonate species could play a role in the kinetics of the ceria-zirconia reduction by CO. Nevertheless, the eventual contribution of the CO adsorption to the rate controlling step should not be disregarded with the available information.

4. Conclusions

In this work, stepwise thermo-gravimetric analysis has been used to determine ultimate CO-OSC and H_2-OSC data for two $Ce_{0.62}Zr_{0.38}O_2$ samples, CZ-MO and CZ-SO, showing significantly different nano-structural and redox properties. Compared to the more usual volumetric approach, stepwise DTG has shown to be a reliable and faster technique for determining this sort of parameter.

As deduced from the results reported here, under both flowing CO and H_2, the CZ-MO sample shows better redox response at all the investigated temperatures. In good agreement with some earlier studies from the literature [25,26,36], the different redox behaviour may be correlated to the nano-structural constitution of the oxides, that showing a pyrochlore-related ordered cationic sub-lattice, CZ-MO sample, being the most reducible one. It should be stressed however, that depending on the temperature, either kinetic or thermodynamic factors may actually determine the recorded ultimate OSC values. As discussed in this work, in the low-temperature range, $T < 773$ K, both CO-OSC and H_2-OSC are kinetically controlled. The role of kinetic factors had already been

established for ultimate H_2-OSC data [25], but not for the analogous parameter determined under flowing CO. Our results also suggest that kinetic limitations are stronger in the case of H_2-OSC measurements. Likewise, our studies on the low-temperature reducibility of CZ-MO and CZ-SO under flowing CO indicate that kinetic restrictions are extended over a wider range of temperatures in the case of the CZ-SO sample.

Acknowledgements

This work has been supported by MEC/FEDER-EU (Project MAT2005-00333) and the Junta de Andalucía (Groups FQM-110 and FQM-334). The ceria-zirconia mixed oxide sample used as starting material in this work was kindly donated by Grace Davison.

References

[1] M. Boaro, A. Trovarelli, J.H. Hwang, T.O. Mason, Solid State Ionics 147 (2002) 85.
[2] A. Trovarelli (Ed.), Catalysis by Ceria and Related Materials, Imperial College Press, London, 2002.
[3] R. Di Monte, J. Kaspar, J. Mater. Chem. 15 (2005) 633.
[4] S. Bernal, G. Blanco, J.J. Calvino, J.M. Gatica, J.A. Pérez Omil, J.M. Pintado, Top. Catal. 28 (2004) 31.
[5] J. Kaspar, P. Fornasiero, N. Hickey, Catal. Today 77 (2003) 419.
[6] M. Shelef, G.W. Graham, R.W. McCabe, in: A. Trovarelli (Ed.), Catalysis by Ceria and Related Materials, Imperial College Press, London, 2002 (Chapter 10).
[7] J. Kaspar, M. Graziani, P. Fornasiero, in: K.A. Gschneidner, L. Eyring (Eds.), Handbook on the Physics and Chemistry of Rare Earths, vol. 29, Elsevier Science B.V., 2000 (Chapter 184).
[8] E. Aneggi, C. de Leitenburg, G. Dolcetti, A. Trovarelli, Catal. Today 114 (2006) 40.
[9] J. Liu, Z. Zhao, C. Xu, A. Duan, L. Wang, S. Zhang, Catal. Commun. 8 (2007) 220.
[10] Z. Zhang, Y. Zhang, Z. Mu, P. Yu, X. Ni, S. Wang, L. Zheng, Appl. Catal. B: Environ. 76 (2007) 335.
[11] J. Mikulova, J. Barbier, S. Rossignol, D. Mesnard, D. Duprez, C. Kappenstein, J. Catal. 251 (2007) 172.
[12] A. Amieiro Fonseca, J.M. Fisher, M.D. Shannon, D. Thompsett, Top. Catal. 44 (2007) 223.
[13] F. Meunier, A. Goguet, C. Hardacre, R. Burch, D. Thompsett, J. Catal. 252 (2007) 18.
[14] K.G. Azzam, I.V. Babich, K. Seshan, L. Lefferts, J. Catal. 251 (2007) 163.
[15] R. Radhakrishnan, R.R. Willigan, Z. Dardas, T.H. Vanderspurt, AIChE J. 52 (2006) 1888.
[16] M. Manzoli, R. Di Monte, F. Boccuzzi, S. Coluccia, J. Kaspar, Appl. Catal. B: Environ. 61 (2005) 192.
[17] A. Martinez-Arias, A.B. Hungria, M. Fernandez-Garcia, J.C. Conesa, G. Munuera, J. Power Sources 151 (2005) 32.
[18] A. Wootsch, C. Descorme, D. Duprez, J. Catal. 225 (2004) 259.
[19] S. Bernal, J.J. Calvino, J.M. Gatica, C. López-Cartes, J.M. Pintado, in: A. Trovarelli (Ed.), Catalysis by Ceria and Related Materials, Imperial College Press, London, 2002 , pp. 85–168 (Chapter 4).
[20] M. Boaro, M. Vicario, C. de Leitenburg, G. Dolcetti, A. Trovarelli, Catal. Today 77 (2003) 407.
[21] P. Fornasiero, R. Di Monte, G. Ranga Rao, J. Kaspar, S. Meriani, A. Trovarelli, M. Graziani, J. Catal. 151 (1995) 168.
[22] R.T. Baker, S. Bernal, G. Blanco, A.M. Cordon, J.M. Pintado, J.M. Rodriguez-Izquierdo, F. Fally, V. Perrichon, Chem. Commun. (1999) 149.
[23] H. Vidal, J. Kaspar, M. Pijolat, G. Colón, S. Bernal, A. Cordón, V. Perrichon, F. Fally, Appl. Catal. B: Environ. 30 (2001) 75.
[24] D. Duprez, C. Descorme, in: A. Trovarelli (Ed.), Catalysis by Ceria and Related Materials, Imperial College Press, London, 2002 , pp. 243–280 (Chapter 7).
[25] M.P. Yeste, J.C. Hernández, S. Bernal, G. Blanco, J.J. Calvino, J.A. Pérez-Omil, J.M. Pintado, Chem. Mater. 18 (2006) 2750–2757.
[26] A. Suda, Y. Ukyo, K. Yamamura, H. Sobukawa, T. Sasaki, Y. Nagai, T. Tanabe, M. Sugiura, J. Ceram. Soc. Jpn. 112 (2004) 586.
[27] N. Hickey, P. Fornasiero, J. Kaspar, M. Graziani, G. Blanco, S. Bernal, Chem. Commun. (2000) 357.
[28] M. Boaro, C. de Leitenburg, G. Dolcetti, A. Trovarelli, J. Catal. 193 (2000) 338.
[29] M. Boaro, F. Giordano, S. Recchia, V.D. Santo, M. Giona, A. Trovarelli, Appl. Catal. B: Environ. 52 (2004) 225.
[30] R. Si, Y.W. Zhang, L.M. Wang, S.J. Li, B.X. Lin, W.S. Chu, Z.Y. Wu, C.H. Yan, J. Phys. Chem. C 111 (2007) 787.
[31] X. Wu, X. Wu, Q. Liang, J. Fan, D. Weng, Z. Xie, S. Wei, Solid State Sci. 9 (2007) 636.
[32] M. Zhao, M. Shen, J. Wang, J. Catal. 248 (2007) 258.
[33] E. Aneggi, M. Boaro, C. de Leitenburg, G. Dolcetti, A. Trovarelli, J Alloys Compd. 408–412 (2006) 1096.
[34] J.C. Hernández, A.B. Hungría, J.A. Perez-Omil, S. Trasobares, S. Bernal, P.A. Midgley, A. Alavi, J.J. Calvino, J. Phys. Chem. C 111 (2007) 9001.
[35] J.A. Pérez-Omil, S. Bernal, J.J. Calvino, J.C. Hernández, C. Mira, M.P. Rodríguez-Luque, R. Erni, N.D. Browning, Chem. Mater. 17 (2005) 4282.
[36] N. Izu, H. Kishimoto, T. Omata, T. Yao, S. Otsuka-Yao-Matsuo, Sci. Technol. Adv. Mater. 2 (2001) 397.
[37] G. Zhou, P.R. Shah, T. Kim, P. Fornasiero, R.J. Gorte, Catal. Today 123 (2007) 86.
[38] C. Mondelli, V. Dal Santo, A. Trovarelli, M. Boaro, A. Fusi, R. Psaro, S. Recchia, Catal. Today 113 (2006) 81.